Effect of Inhomogeneous Medium on Fields above GCPW PCB for Near-Field Scanning Probe Calibration Application

Shubhankar Marathe, *Student Member, IEEE,* Hamed Kajbaf, *Senior Member, IEEE,* Morten Soerensen, *Member, IEEE,* Victor Khilkevich, *Member, IEEE,* David Pommerenke, *Fellow, IEEE,* Jin Min, and Giorgi Muchaidze

***Abstract*—In this paper, a method is proposed to calibrate a probe by placing it into a known field and referencing its output voltage to the known field. A transmission line is a convenient structure for creating such a known field. This paper presents the effect of the inhomogeneous medium on the near-field generated over a grounded coplanar waveguide (GCPW) PCB and reports the field pattern over the GCPW. GCPW PCB's are used to determine the probe factor for near-field scanning applications. A near-field scan is performed to visualize the near-field sources over a DUT. The near-field is measured by using E- and H-field EMI probes. The output of these probes is a voltage and using the probe factor, the field present over the DUT can be determined. To calculate the probe factor, the near-field strength needs to be known using 3D simulation. GCPW creates a quasi-TEM field. The effect of non-TEM modes is easily underestimated, such that non-TEM fields prevent the user from determining the unwanted field suppression of probes at higher frequencies.**

***Index Terms*—E-field probe, GCPW, H-field probe, near-field scanning, probe calibration.**

I. Introduction

NEAR-FIELD scanning is used to visualize the near-field sources present inside an electronic device. The near-fields are measured using near-field E and H probes. The probes can have a broadband frequency response or a resonant narrowband response. The resonant probes have a higher signal to noise ratio in the narrowband frequency range than the broadband probes. The near-field data obtained using the probes [1]-[3] is valuable; for example, identifying radio frequency interference (RFI) in mobile devices. One of the applications of the near-field scanning technique is to generate models of ICs or emission sources on PCBs by obtaining the near-field data over the device under test (DUT). This data along the Huygens' surface can be utilized for far-field estimation [4], and for source reconstruction-based investigations [5]. The emission frequency spectrum may range from a few KHz up to 40 GHz and higher. Recent developments in 5G wireless communication and testing have introduced the usage of 20 GHz and higher frequency spectrums [6]-[8] which has created the need for high-frequency near-field scanning probes and their calibration. A few other applications include optical transceivers, harmonics generated from PCI-E on-board, etc., where scanning at 20 GHz and higher frequencies is desirable.

Manuscript received Feb. 7, 2018. This work was supported in part by the National Science Foundation under Grant IIP-1440110.

S. Marathe, M. Soerensen, V. Khilkevich, and D. Pommerenke are with the EMC Laboratory, Missouri University of Science and Technology, Rolla, MO 65401 USA (e-mail: skmcr4@mst.edu; sorensenmo@mst.edu; khilkevichv@mst.edu; davidjp@mst.edu).

H. Kajbaf, J. Min, and G. Muchaidze are with the Amber Precision Instruments, Sunnyvale, California, USA (email: hamed@amberpi.com jinmin@amberpi.com; giorgi@amberpi.com).

The concept of probe factor calibration refers to the calibration of the voltage at the probe output in a field that is disturbed by the probe, relative to the field which is present without the probe. This way, the effect of the probe on the field is taken into account. The probes usually do not measure the field when the probe is present, but the field which was there before the probe was inserted. Various probe calibration methods are published in literature, for example, a low-frequency probe calibration using the Helmholtz coil (typically from 9 KHz to 10 MHz) and the TEM cell (typically from 9 KHz to 1000 MHz) or the GTEM cell (typically from 9 KHz to 1 GHz) [9]-[11] or free field calibration using horn antennas. A few other methods mentioned in the IEEE Std. 1309-2013 [11], also include open-ended waveguide (typically from 200 MHz to 450 MHz) and the pyramidal horn antennas (typically from 450 MHz to 40 GHz). The goal of this research is to identify a single probe calibration method, which can work for large frequency bandwidth. From the available choices, the GCPW transmission line is selected as it supports wide frequency bandwidth and due to its convenience of measuring the field strength over small heights over the trace structure.

The probe factor calculation steps involve calculating the field strength (using 3D simulation) above a microstrip or a GCPW PCB based on the desired frequency range of interest. Applying a source excitation to the microstrip or GCPW PCB and placing the near-field probe at the desired height over the PCB by using high precision robot scanning system [12]. Measurement cables, amplifiers, attenuators can be included in the calibration procedure. The voltage measured using VNA will be referenced to the simulated field strength, and the probe factor or the system factor is calculated. Probe factor is called as system factor when the measurement components like the cables, amplifiers, attenuators, etc., are included in the measurement set-up. The simulated fields obtained from the simulation model are important to accurately calculate the probe factor [13]. The probe factor for E- or H-field can be given by:

$$PF = \frac{E\,or\,H_{simulated}(f, h_{eff})}{S_{21}.V_{simulated}} \quad (1)$$

where the E- or the H-field is obtained from simulation at a fixed frequency f, at an effective height h_{eff} above the surface

of the trace. The $V_{simulated}$ refers to the voltage applied at the trace in the simulation model, which generated the simulated E or H-field above the trace. The S_{21} is obtained from the measurement as shown in Fig. 1. An accurate probe factor calibration leads to an accurate estimation of the measured field strength over the DUT. An illustration of the probe factor calibration measurement setup is shown in Fig. 1.

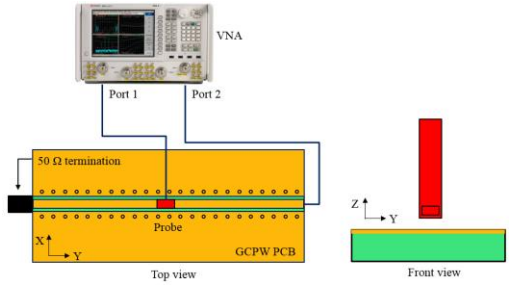

Fig. 1. Measurement set-up for probe factor calculations using a GCPW PCB.

One of the applications of these calibration structures is to quantify the undesired field component suppression for a near-field probe. For instance, for an H-field probe placed above the GCPW calibration structure shown in Fig. 1, the desired (TEM) component is the H_x field component and the H_y is the undesired (non-TEM) field component. The y-component is along the wave propagation direction and, hence, in a quasi-TEM wave geometry, the component is expected to be much smaller than the desired component. In such applications, if the fields generated by the calibration structure itself have stronger non-TEM or the undesired fields, then it makes the calibration structure unsuitable for probe undesirable field component suppression quantification measurements.

At first glance, one may believe that the field structure over a GCPW or microstrip is not a function of frequency as the structure supports a quasi-TEM wave. This paper discusses the effect of the inhomogeneous medium in GCPW PCB. At first it was assumed that a GCPW transmission line would have a TEM-dominated fields above the PCB for the desired frequency range. From the simulated near-field data, it was found that that this assumption does not hold true. A difference in the maximum field strength, asymmetric field variation on the two sides of the trace, and magnitude variation along the length of the trace were observed. One of the core findings is that the variation of the desired component (about 3-8 dB) along the length of the trace at about 30 GHz and higher frequencies suggests that the during the calibration process, the position of the near-field scanning probe becomes important. If the probe is not placed at the center of the length of the GCPW where the simulated field is determined, then the fields measured by the probe will not lead to an offset of 3-8 dB in the field strength calculation based on the probe factor (1) calculation using the simulation and the measurement. The variation in the desired component along the length of the trace can be reduced by reducing the PCB thickness [14], thus, by keeping the cross-sectional waveguide geometry electrically small for the highest frequency of interest.

The GCPW PCB was simulated using CST MWS [15] and the effect of the inhomogeneous medium on the near-field x-component (perpendicular to the trace) of the E- and H-field are reported. With the increase in frequency, the height above the GCPW PCB, which can be utilized for probe factor measurements, is restricted. The investigation in this paper was performed up to 40 GHz on a RO4350 dielectric based GCPW PCB. To confirm the effect of the inhomogeneous medium, a GCPW PCB with air as the dielectric material was simulated and compared to the RO4350 dielectric material. Here, the comparisons are quantified using the ratio of the desired (TEM) and the undesired field (non-TEM) component at a particular frequency and a fixed scanning height above the trace surface.

II. GCPW SIMULATION MODEL

The two simulation models were used to determine if the unwanted field variations were caused by the launch section (connector-PCB transition) or a result of the non-TEM field due to the inhomogeneous dielectric medium interface. First, a GCPW with RO4350 low-loss dielectric structure was investigated. Then an only-air dielectric GCPW was simulated to observe the difference between the air-air interface and the RO4350-air interface in the RO4350-based GCPW PCB.

The 0.762 mm RO4350 dielectric material-based GCPW PCB available from Southwest Microwave [16] was used as a typical low-loss high-frequency board. These boards are typically used for signal integrity applications, which was not the focus of this study. In this application, it was used as an intentional near-field source for probe factor calibration applications. For reducing the simulation time, the stitching ground vias are modeled as rectangular blocks in the CST MWS model. It is important to note that the frequency dependence of the RO4350 dielectric material was considered in the simulation model and is illustrated in Fig. 3. The time domain solver based on finite integration technique (FIT) was used for solving the model with a Gaussian excitation source applied at the waveguide ports placed at the GCPW connectors. The model has around 6 million hexahedral mesh cells and the time domain accuracy is increased to -60 dB to achieve better convergence in the simulated results.

Another simulation model was designed for the same structure, but instead of the RO4350 dielectric, the PCB was designed using air dielectric. To maintain similarity to the RO4350 PCB, only the air dielectric substrate was changed to obtain the nominal 50 Ω trace impedance in the simulation model. The substrate thickness was reduced from 0.762 mm to about 0.249 mm for air as the dielectric. Table I provides the design parameters of the two GCPW geometries considered for the desired near-field component investigation.

The E- and H-field monitors were defined for a volume in the CST models, and the field magnitude was determined for the frequency range from 0.1 GHz to 40 GHz. The simulated results are analyzed by plotting the field magnitude at the center of the PCB width along the length of the PCB as shown in Fig. 2 (a). In addition, the near-fields are analyzed at the center of the PCB length, along the width of the PCB respectively as shown in Fig. 2 (b). The trace surface is considered as 0 mm reference height. The desired x-component is plotted over the solid line as shown in the Figs. 2 (a) and 2 (b). The analysis was performed at different heights above the trace surface such as 1 mm, 2 mm above the trace, etc. It should be noted that in Fig. 2, the evaluation line is shown for 1 mm above the trace surface.

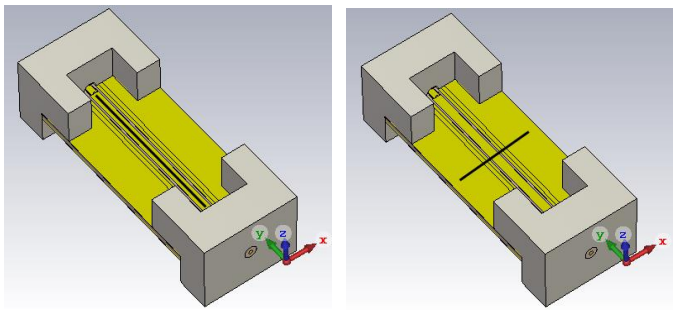

(a) (b)

Fig. 2. The simulation model of the RO4350 dielectric based GPCW PCB with connector model. (a) The solid line represents the field plotted at the center of the width of the PCB but along the length of the PCB or the trace (y-direction). (b) The solid line represents the field plotted at the center of the PCB length but along the width of the PCB or the trace (x-direction).

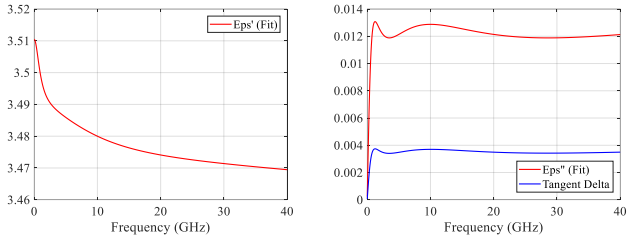

(a) (b)

Fig. 3. The frequency dependence of the RO4350 dielectric material properties used in the simulation model. For the electric dispersion, the Nth order model with N=3 (constant tangent delta fit) is used in the simulation. (a) Eps' or the dielectric constant (b) Eps" and the tangent delta.

TABLE I: DESIGN PARAMETERS OF THE TWO GCPW MODELS INVESTIGATED USING CST MWS SIMULATION

Design	PCB Length	PCB Width	Trace width	Top ground gap	Substrate	Substrate thickness
Rogers 4350-based GCPW	25.4 mm	12.7 mm	1.143 mm	0.241 mm	RO4350, $\varepsilon_r(f) = 3.48$	0.762 mm
Air dielectric GCPW	25.4 mm	12.7 mm	1.143 mm	0.241 mm	Air, $\varepsilon_r = 1$	0.249 mm

III. Simulation Results

The GCPW structure implemented in a RO4350 PCB dielectric and air on the trace top surface is expected to have quasi-TEM mode because the wave propagation velocity in dielectric and air are different, which leads to a quasi-TEM mode. The GCPW structure with air dielectric is expected to have TEM mode because of the homogeneous medium for the wave propagation.

The y-direction is along the length of the trace, the x-direction is perpendicular to the trace. The x-component of the E- and H-fields are the desired field components for the probe factor calibration calculation. In this Section, the field components are shown at different heights above the trace, frequency, along the width of the trace, and along the length of the trace. The main finding here is that as frequency increases, the desired E_x or the H_x field component has ripples or variations along the length of the trace, for example, the 0.762 mm thick RO4350 GCPW. On the contrary, the PCB geometry with 0.249 mm thick air dielectric GCPW observes much lesser variation along the length of the trace. The variation along the length of the trace can be reduced by making the PCB thinner, thus, keeping the cross-sectional waveguide geometry electrically small for the highest frequency of interest.

The simulation results for the RO4350 dielectric and the air dielectric are compared for the desired H_x and the E_x component. The magnitude of the two components is plotted along the length of the PCB (y-direction) and along the width (x-direction) of the PCB at y equal to 0 mm (center position of the trace length). In the following plots the effect of the frequency at a fixed height of z = 1 mm is observed. Later the effect of height will be considered. The desired H_x component at a height of z = 1 mm above the GCPW PCB for the RO4350 dielectric based model is plotted in the Fig. 4 and Fig. 5.

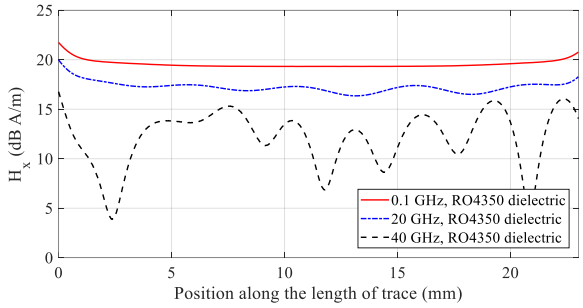

Fig. 4. Desired H_x component over the RO4350 GCPW trace along the length (y-direction, parallel to the trace) of the PCB at 0.1, 20 and 40 GHz. Note the strong reduction of the field for 40 GHz compared to Fig. 6.

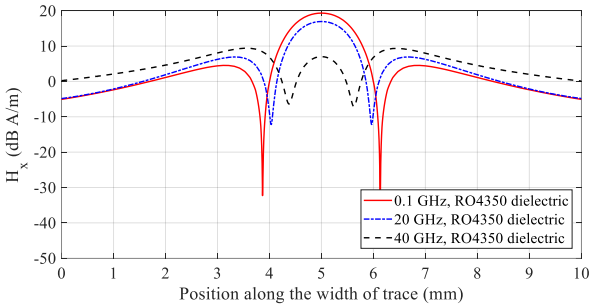

Fig. 5. Desired H_x component over the RO4350 GCPW trace along the width (x-direction) of the PCB at 0.1, 20 and 40 GHz. The curve length of 5 mm represents the center position of the PCB trace width. Note the strong reduction of the field for 40 GHz compared to Fig. 7.

Fig. 5 shows about a 12 dB variation at the center of the trace width (5 mm) at 40 GHz for the H_x component at a height of z = 1 mm above the GCPW PCB. The desired H_x component at a height of z = 1 mm above the GCPW PCB for the air dielectric-based model is plotted in the Fig. 6 and Fig. 7.

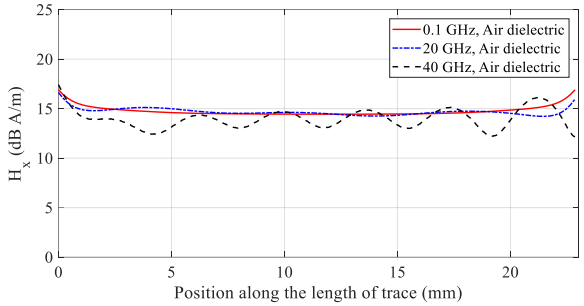

Fig. 6. Desired H_x component over the air GCPW trace along the length (y-direction) of the PCB at 0.1, 20, and 40 GHz. The y-axis scale is kept to the same range as in Fig. 4 for better comparison.

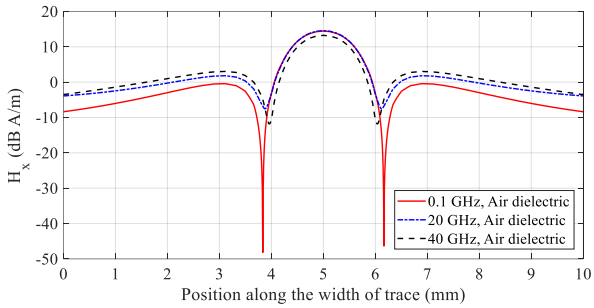

Fig. 7. Desired H_x component over the air GCPW trace along the width (x-direction) of the PCB at 0.1, 20, and 40 GHz. The curve length at 5 mm represents the center position of the PCB trace width. Note that the field is only a weak function of frequency verifying the TEM behavior of the fields.

Referencing the probe factor calibration application, it is observed that the magnitude component in Fig. 4 has a large variation from 0.1 GHz to 40 GHz when compared to the plots in Fig. 6. The magnitude difference is within 1-2 dB up to 20 GHz, but there are about 14 dB variations at 40 GHz along the length of the PCB in Fig. 4. Compared to the simulation results obtained using the air dielectric model, the magnitude variation along the length of the PCB is within 4 dB for the frequencies from 0.1 to 40 GHz in Fig. 6. The variation in amplitude for the air dielectric is much less than the RO4350 dielectric which suggests the probe height over the PCB is important while performing the probe factor measurements using a RO4350 dielectric material GCPW. The peak magnitude value for the air dielectric simulation model varies only by 1.5 dB, as shown in Fig. 7, confirming that this is a TEM wave. For the commercially available GCPW PCB's such as the RO4350 dielectric based-model a variation of 12 dB is observed as shown in Fig. 5.

The near-field desired E_x component is analyzed similarly along the length and the width of the PCB. The E_x component at a height of z = 1 mm above the GCPW PCB for the RO4350 dielectric-based model is plotted in Fig. 8 and Fig. 9. In addition, the desired E_x component at a height of z = 1 mm above the GCPW PCB for the air dielectric-based model are plotted in the Fig. 10 and Fig. 11.

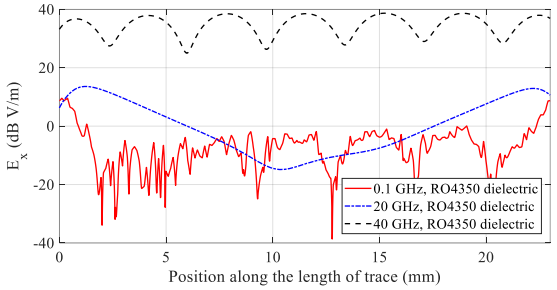

Fig. 8. Desired E_x component over the GCPW trace along the length (y-direction) of the PCB at 0.1, 20, and 40 GHz but exactly in the middle where the component has a null. Note the strong values for 40 GHz compared to Fig. 10.

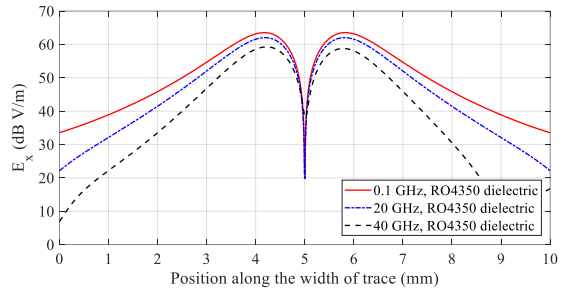

Fig. 9. Desired E_x component over the GCPW trace along the width (x-direction) of the PCB at 0.1, 20, and 40 GHz. The curve length of 5 mm represents the center position of the PCB trace width.

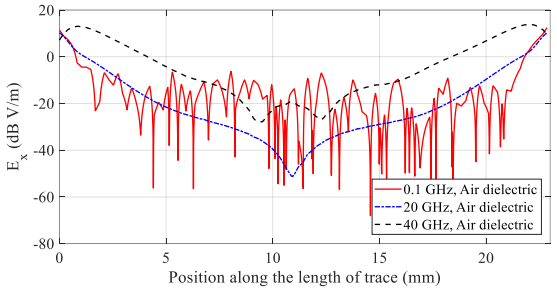

Fig. 10. The E_x component over the GCPW trace along the length (y-direction) of the PCB at 0.1, 20 and 40 GHz. Note that the unwanted longitudinal component is mainly excited at the connector transition.

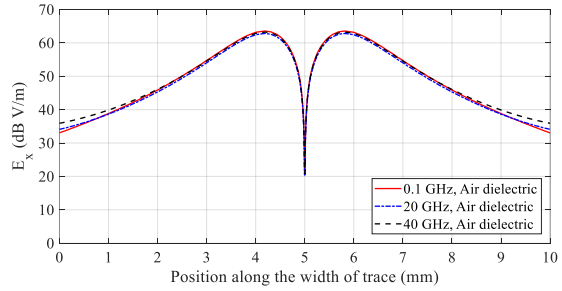

Fig. 11. The E_x component over the GCPW trace along the width (x-direction) of the PCB at 0.1, 20 and 40 GHz. The curve length of 5 mm represents the center position of the PCB trace width. Note that the frequency independence again is an indication for the dominance of the TEM mode.

Fig. 10 shows the desired field at the center of the trace where the component has a null for the air GCPW; the field strength variation is about -10 to -40 dB. The desired E_x component has the strongest magnitude around the edges of the PCB trace width which is about 63 dB in Fig. 11. Hence, the null field strength is much less than the peak magnitude field strength and the noise floor looking waveforms in the Fig. 8 and Fig. 10 can be considered acceptable based on the simulated near-field waveforms.

IV. Testing The Rejection Ratio Of A Near-Field Probe

Every H-field probe is sensitive to E-field and vice versa, also a H_x probe cannot perfectly reject other magnetic field components. A typical way to determine the rejection ratio of a H_x probe would be to place the probe at first in the middle of the trace and rotate it to the desired field component (H_x) to obtain a reference reading. Then, the probe is rotated by 90 degrees, assuming that the desired component is perfectly rejected and that no longitudinal component exists (H_y), as one would expect in a TEM wave. In this case, the remaining signal picked up by the probe would only be caused by the electric field coupling.

This numerical simulation allows testing the underlying assumption of not having a longitudinal H_y component. It is known that magnetic field probes are sensitive to the E-field especially if they are offset to the side of the trace and rotated into an orientation in which they reject the TEM field. However, the conclusion could be wrong, if the non-TEM field is stronger on the side of the trace. In this case, the probe would couple to the non-TEM field, but the user may misinterpret this as coupling to the E-field. To investigate this, the non-TEM fields were also plotted to the side of the trace and compared to the desired field component. It is important to note that the numerical simulation allows for identifying the desired quasi-TEM or the TEM components (H_x, H_z, E_x, and E_z) and the non-TEM components (H_y and E_y). The following plots give an insight into the field rejection ratio, which is defined as:

$$H-Field\ Rejection\ Ratio = \frac{H_x(f, h_{eff})}{H_y(f, h_{eff})} \quad (2)$$

$$E-Field\ Rejection\ Ratio = \frac{E_x(f, h_{eff})}{E_y(f, h_{eff})} \quad (3)$$

In this rectangular co-ordinate system, the x- and z-components are the desired TEM field components and the y-component is the undesired non-TEM field component. The field rejection ratio is defined as the field strength of the desired component at an expected maximum location divided by the maximum field strength of the undesired field component. For instance, the expected maximum H_x field will be at the center of the trace width, and at the edge of the trace width for the E_x field component as shown in Fig. 7 and Fig. 11, respectively. Using this definition, the field rejection ratios are determined and illustrated in Figs. 12 to 15.

A. *Comparison between the two GCPW generated fields at a fixed height and frequency*

In Fig. 12 and Fig. 13 the rejection ratio of the RO4350 dielectric-based GCPW generated fields are compared. Fig. 12 shows the plot of the quasi-TEM H_x and the non-TEM H_y along the width of the trace.

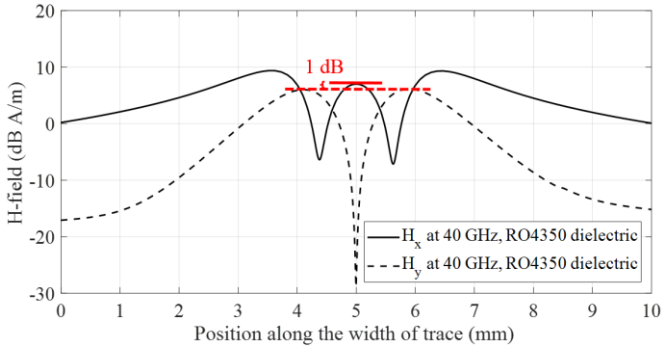

Fig. 12. Side scan comparison of the desired H_x component (solid line) and the non TEM H_y component (dashed line) over the RO4350 GCPW trace along the width (x-direction) of the PCB at z = 1 mm at 40 GHz. Note that at 1 mm the maximum of the non-TEM component is only 1 dB below the maximum of the desired component.

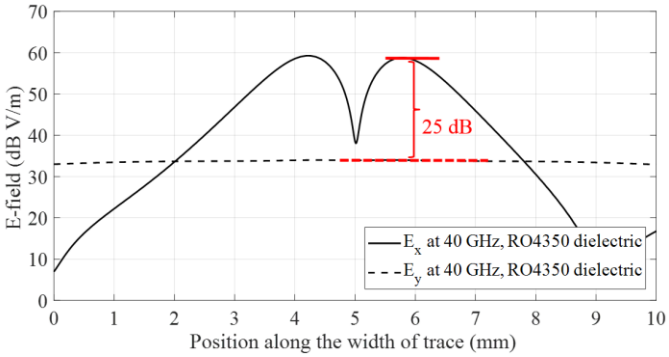

Fig. 13. Side scan comparison of desired E_x component (solid line) and the E_y component (dashed line) over the RO4350 GCPW trace along the width (x-direction) of the PCB at z = 1 mm at 40 GHz.

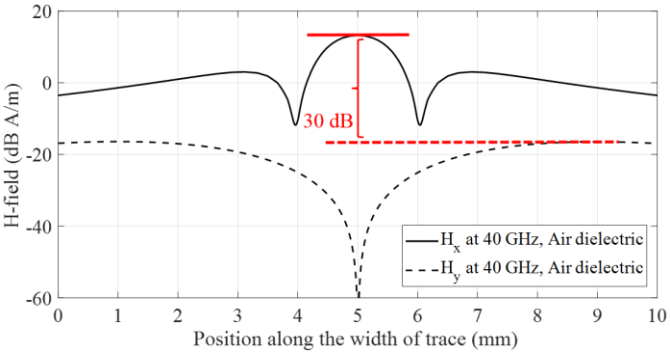

Fig. 14. Side scan comparison of the desired H_x component (solid line) and the non TEM H_y component (dashed line) over the air GCPW trace along the width (x-direction) of the PCB at z = 1 mm at 40 GHz. Note that at 1 mm the maximum of the non-TEM component is 30 dB below the maximum of the desired component.

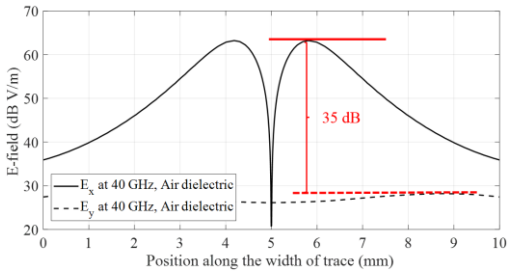

Fig. 15. Side scan comparison of desired E_x component (solid line) and the E_y component (dashed line) over the air GCPW trace along the width (x-direction) of the PCB at z = 1 mm at 40 GHz. Note that at 1 mm the maximum of the non-TEM component is 35 dB below the maximum of the desired component.

On comparing the Figs. 12 and 14, it is observed that the non-TEM component at 40 GHz in the RO4350 dielectric GCPW is only 1 dB weaker than the desired H_x field. This is a strong indication of the inhomogeneous medium effect on the near-field above the PCB geometry. In the case of the air dielectric GCPW as shown in Fig. 14, the non-TEM component is 30 dB weaker than the desired field component. This quantification of the rejection ratio of the fields generated by the characterization PCB geometry is an important factor in determining the rejection ratio of a near-field scanning probe during probe characterization or evaluation measurements. Similarly, the behavior is seen in the E-field plots in Fig. 13 and Fig. 15. The air dielectric GCPW has effectively 35 dB weaker non-TEM field component, as compared to the 25 dB suppression in the RO4350 dielectric GCPW at z = 1 mm at the highest frequency of interest.

B. Comparison between the two GCPW generated fields at a fixed frequency and different heights

In Fig. 16 and Fig. 17, the desired H_x and the undesired (non-TEM) H_y components are plotted along the width of the trace at scanning heights of 1 mm and 2 mm at 40 GHz frequency. Fig. 16 shows the results for the RO4350 GCPW trace, where it is seen that the H_y component changes with the scanning height. However, it is observed in Fig. 17 for the air GCPW, the H_y (non-TEM) component does not increase in magnitude when the scanning height is changed from 1 mm to 2 mm. A similar effect is observed for the E-field in Fig. 18 and Fig. 19, however, a small increase is observed in the E_y field component. The increase in the undesired y-component is shown by the red dashed lines in the Figs. 16 to 19.

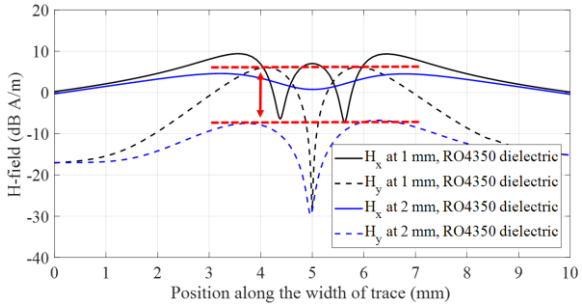

Fig. 16. Side scan comparison of the desired H_x component (solid line) and the H_y component (dashed line) over the RO4350 GCPW trace along the width (x-direction) of the PCB at z = 1 mm and 2 mm at 40 GHz.

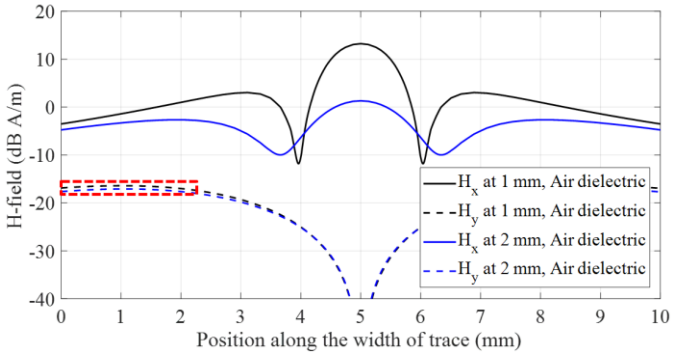

Fig. 17. Side scan comparison of desired H_x component (solid line) and the H_y component (dashed line) over the air GCPW trace along the width (x-direction) of the PCB at z = 1 mm and 2 mm at 40 GHz.

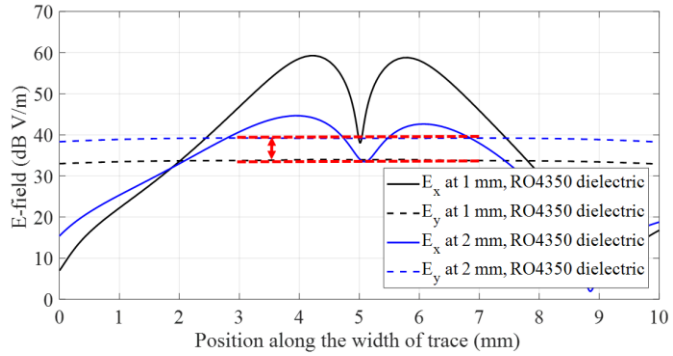

Fig. 18. Side scan comparison of desired E_x component (solid line) and the undesired E_y component (dashed line) over the RO4350 GCPW trace along the width (x-direction) of the PCB at z = 1 mm and 2 mm at 40 GHz.

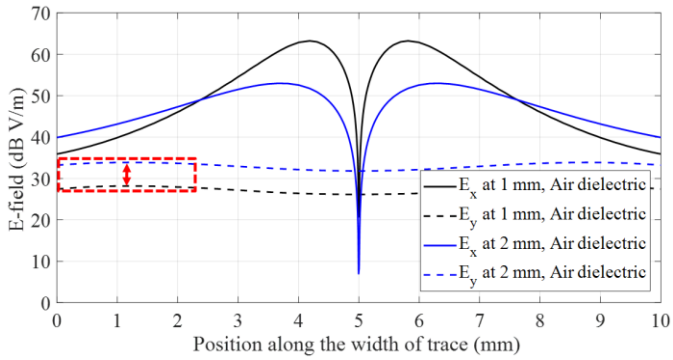

Fig. 19. Side scan comparison of desired E_x component (solid line) and the undesired E_y component (dashed line) over the air GCPW trace along the width (x-direction) of the PCB at z = 1 mm and 2 mm at 40 GHz.

Table II lists the rejection ratios calculated using (2) and (3) for various frequencies. The table shows the trend that as the frequency of interest increases, the undesired (non-TEM) H_y field component magnitude becomes comparable to the desired H_x field strength. Referencing the near-field scanning applications at higher frequencies, the inhomogeneous dielectric-based GCPW is not suitable for generating the desired quasi-TEM waves. For instance, at 40 GHz frequency the rejection ratio for the H-field (H_x/H_y) when using the

RO4350 GCPW is only 1 dB. However, an air dielectric GCPW provides about 30 dB non-TEM (H_y) component suppression.

TABLE II: FIELD REJECTION RATIO FOR VARIOUS FREQUENCIES FOR RO4350 AND AIR DIELECTRIC GCPW AT 1 MM ABOVE THE TRACE

Frequency	For RO4350 GCPW = H_x/H_y	For Air GCPW = H_x/H_y	For RO4350 GCPW = E_x/E_y	For Air GCPW = E_x/E_y
0.1 GHz	57 dB	54 dB	69 dB	62 dB
10 GHz	18 dB	44 dB	50 dB	43 dB
20 GHz	13 dB	49 dB	37 dB	38 dB
30 GHz	10 dB	42 dB	49 dB	45 dB
40 GHz	1 dB	30 dB	25 dB	35 dB

V. Discussion And Conclusion

The CST MWS simulation was performed on the grounded coplanar waveguide PCB designed using the RO4350 dielectric. At higher frequencies, stronger non-TEM field components were observed, such that the suppression between the quasi-TEM and the non-TEM is only about a few dB as shown in Table II for the 40 GHz frequency for the H-field.

The desired x-component of the E and H-fields were simulated over the RO4350 GCPW trace structure. The x-component of the E- or H-field is plotted on a line at a fixed height, along the length of the trace at 0.1 GHz, 20 GHz, and 40 GHz. In this RO4350 GCPW structure, the air and RO4350 dielectric are the two media through which the waves propagate. To verify the effect of the inhomogeneous medium on the field above the PCB, another set of simulations were performed by replacing the RO4350 dielectric with air as a dielectric medium.

These simulations revealed that while performing the near-field probe calibration or calculating the probe factor of a near-field probe, the effect of the inhomogeneous media needs to be taken in to account to determine the effective height and the frequency range supported by the GCPW PCB; for example, Fig. 12 illustrates this effect. In addition, for the near-field probe rejection ratio calculation using (2) and (3), the near-field generating PCB must be well evaluated for the presence of the non-TEM field components at the desired height; for example, 1 mm above the surface. It is important that the rejection ratio of the near-field generating source PCB should be more than the value obtained for a near-field scanning probe during its probe undesired field suppression measurements. This criterion ensures that, for example, an H-field probe's unwanted measured component was the E-field coupling and not the non-TEM component generated by the calibration PCB.

The simulation results reveal that using an air dielectric GCPW geometry provides better field rejection ratio than the RO4350 dielectric based GCPW. The field rejection values for the E- and H-field are provided in Table II. An air dielectric structure generates the desired TEM fields, which are important for the near-field probe factor calibration measurement application.

References

[1] G. Li, K. Itou, Y. Katou, N. Mukai, D. Pommerenke, and J. Fan, "A resonant E-field probe for RFI measurements," *IEEE Trans. EMC*, vol. 56, no. 6, pp. 1719-1722, 2014.

[2] E. Song and H. H. Park, "A high-sensitivity electric probe based on board-level edge plating and LC resonance," IEEE Microw. Wireless Compon. Lett., vol. 24, no. 12, pp. 908–910, Dec. 2014.

[3] S. Shinde, S. Marathe, G. Li, R. Zoughi and D. Pommerenke, "A Frequency Tunable High Sensitivity H-field Probe Using Varactor Diodes and Parasitic Inductance," *IEEE Trans. Electromagn. Compat.*, vol. 58, no. 1, pp. 331-334, February 2016.

[4] H. Weng, D. G. Beetner, and R. E. DuBroff, "Prediction of radiated emissions using near field measurements," IEEE Trans, Electromagn. Compat., vol. 53, no. 4, pp. 891–899, Nov. 2011.

[5] Y. Alvarez, M. Rodriguez, F. Las-Heras, and M. Hermando, "On the use of the source reconstructing method for estimating radiated EMI in electronic circuits," IEEE Trans. Instrum. Meas., vol. 59, no. 12, pp. 3174– 3183, Dec. 2010.

[6] Y. Qi, G. Yang, L. Liu, J. Fan, A. Orlandi, H. Kong, W. Yu, and Z. Yang, "5G Over-the-Air Measurement Challenges: Overview," *IEEE Trans. Electromagn. Compat.*, vol. 59, no. 6, pp. 1661-1670, Dec. 2017.

[7] T. S. Rappaport, G. R. MacCartney, M. K. Samimi, and S. Sun, "Wideband millimeter-wave propagation measurements and channel models for future wireless communication system design," IEEE Transactions on Communications, vol. 63, no. 9, pp. 3029–3056, Sept 2015.

[8] T. Wheeler, "Leading towards next generation "5g" mobile services," August 2015. [Online]. Available: https://www.fcc.gov/news-events/blog/2015/08/03/leading-towardsnext-generation-5g-mobile-services

[9] R. A. Pahl, J. L. Rovey, D. J. Pommerenke, "Calibration of magnetic field probes at relevant magnitudes," in 19th IEEE Pulsed Power Conference (PPC), pp. 1–6, June 2013.

[10] W. Huang, D. Liu, J. Xiao, D. Pommerenke, J. Min, and G. Muchaidze, "Probe characterization and data process for current reconstruction by near field scanning method," in Proc. Asia-Pacific Symp. Electromagn. Compat. (APEMC), Apr. 2010, pp. 467–470.

[11] IEEE Standard for Calibration of Electromagnetic Field Sensors and Probes (Excluding Antennas) from 9 kHz to 40 GHz, 2013.

[12] Smart Scan EMI 350 Series. 2016. [Online]. Available: http://www.amberpi.com/

[13] J. Zhang, K. W. Kam, J. Min, V.V. Khilkevich, D. Pommerenke, and J. Fan, "An effective method of probe calibration in phase resolved Near-field scanning for EMI application," *IEEE Trans. Instrum. Meas.*, vol. 62, no. 3, pp. 648-658, March 2013.

[14] M. Soerenson, S. Marathe, D. Pommerenke, J. Min, and H. Kajbaf, "Design of TEM Transmission Line for Probe Calibration up to 40 GHz," 2018 IEEE Symposium on Electromagnetic Compatibility & Signal/Power Integrity (EMCSI)-to appear.

[15] CST Microwave studio. 2016. [Online]. Available: https://www.cst.com/

[16] Optimizing Test Boards for 50 GHz End Launch Connectors. 2016. [Online]. Available: http://mpd.southwestmicrowave.com/resources/

Shubhankar Marathe (S'14) received a B.E. degree in Electronics and Telecommunication from the University of Mumbai, Mumbai, Maharashtra, India in 2013, and an M.S. degree in Electrical Engineering from the Missouri University of Science and Technology, Rolla, Missouri, USA in 2017. He is a Ph.D. candidate in Electrical Engineering at the EMC Laboratory, Missouri University of Science and Technology, Rolla, Missouri, USA.
In 2016, he was a Hardware Engineer Intern at Cisco Systems, RTP, NC, USA. His research interests include Near-Field Scanning, Electrostatic Discharge, EMC Measurements and Signal Integrity.

Hamed Kajbaf (S'08-M'12-SM'18) received the BS degree in electrical engineering from Shiraz University, Shiraz, Iran, in 2006 and he received the MS degree in biomedical engineering-bioelectric from Tarbiat Modares University, Tehran, Iran, in 2009. He received the PhD in electrical engineering from Missouri University of Science and Technology, Rolla, MO, in 2012.
He has previously worked at SpaceX as EMC Design Engineer. He is currently a Principal EMC Engineer at Amber Precision Instruments, San Jose, CA. His research interests include RF instrumentation, EMC and microwave scanning systems, near-field electromagnetic and acoustic measurement, and array signal acquisition/processing.

Morten Soerensen (M'08) received a M.S degree in Physic from Aarhus University, Aarhus, Denmark in 2004. From 2006 to 2017 he was Antenna & EMC specialist at Bang & Olufsen, Denmark including 3 years (2011-2014) as researcher and technical project manager in the innovation consortium, "EMC Design – First Time Right". In 2017 he joined the EMC Laboratory, Missouri University of Science and Technology, Rolla, MO, USA where he is visiting assistant research profesor and from 2018 he has been part time with Amber Precision Instruments. His current resarch interests include near-field scanning, electrostatic discharge and system-level radiated emission.

Victor Khilkevich (M'08) received the Ph.D. degree in electrical engineering from the Moscow Power Engineering Institute, Technical University, Moscow, Russia, in 2001.
He is currently an Assistant Professor at the Missouri University of Science and Technology, Rolla, MO, USA. His primary research interests include microwave imaging, automotive electromagnetic compatibility modeling, and high-frequency measurement techniques.

David Pommerenke (F'15) received a Ph.D. degree from the Technical University of Berlin, Berlin, Germany, in 1996. After working with Hewlett Packard for five years, in 2001 he joined the EMC Laboratory, Missouri University of Science and Technology, Rolla, MO, USA, where he is currently a Professor. His current research interests include System-Level ESD, Electronics, Numerical Simulations, EMC Measurement Methods, and Instrumentation.
Dr. Pommerenke is an Associated Editor for the IEEE transaction on EMC. He has authored or coauthored more than 200 papers, co-owner of a start-up company on EMC scanning and is the inventor on 13 patents.

Kyungjin "Jin" Min received the Ph.D. degree from the North Carolina State University, in 1998. After working at LSI Logic and Perkin Elmer for four years, he co-founded Global Technology Leader in 2004, and co-founded Amber Precision Instruments in 2006, where he is responsible for operations and technology development. His interests are development of EMC scan technologies and EMC scanners. He has authored and co-authored more than 20 publications and holds six patents. He was a member of ESDA (Electrostatic Discharge Association) Standard Committee, involving component ESD and LU test standard revision and JEDEC and ESDA joint standard preparation.

Giorgi Muchaidze received the B.S.M.E. and M.S.C.S. degrees from the Georgian Technical University, Tbilisi, Georgia, in 1996 and 2002, respectively, and the M.S.E.E. degree from the Missouri University of Science and Technology, Rolla, in 2007.

He was at the EMCoS Consulting and Software Company, Georgia. In 2005, he joined the Electromagnetic Compatibility Laboratory, Missouri University of Science and Technology, Rolla. Since 2007, he has been with Amber Precision Instruments, San Jose, CA. His current research interests include system-level immunity testing and EMC/EMI measurements.